Multifunctional Biocomposites Based on Polyhydroxyalkanoate and Graphene/Carbon Nanofiber Hybrids for Electrical and Thermal Applications

DOI:
10.1021/acsapm.0c00539

Document Version
Accepted author manuscript

Multifunctional Biocomposites based on Polyhydroxyalkanoate and Graphene/Carbon-Nanofiber Hybrids for Electrical and Thermal Applications

Pietro Cataldi, Pietro Steiner, Thomas Raine, Kailing Lin, Coskun Kocabas, Robert J. Young, Mark Bissett, Ian A. Kinloch*, Dimitrios G. Papageorgiou*†*

Department of Materials and National Graphene Institute, University of Manchester, Oxford Road, Manchester, M13 9PL UK
† School of Engineering and Materials Science, Queen Mary University of London, Mile End Road, London E1 4NS, UK

* Corresponding authors e-mails: pietro.cataldi@manchester.ac.uk, d.papageorgiou@qmul.ac.uk, ian.kinloch@manchester.ac.uk

Abstract

Bio-based and/or biodegradable plastics have been proposed as a sustainable alternative to long lasting and fossil fuel derived ones. Amongst those available, polyhydroxyalkanoate (PHA) shows great potential across a large variety of applications but it is not used extensively due to its relatively poor physical properties. An expansion of its uses can be accomplished by developing nanocomposites where PHAs are utilised as the polymer matrix. Herein, a PHA biopolyester was melt blended with graphene nanoplatelets (GNPs) or with a hybrid mixture of GNPs and carbon nanofibers. The resulting nanocomposites exhibited enhanced thermal stability and satisfactory mechanical properties. The hybrid nanocomposites percolated electrically at lower nanofiller loadings compared to the GNP-PHA system. The electrical conductivity at 15 wt.% loading was ~ 6 times higher than the GNP-based nanocomposite. As a result, the electromagnetic interference shielding performance of the hybrid material was around 50% better than the pure GNP-reinforced nanocomposites. The thermal conductivity increased significantly for both types of bio-nanocomposites and reached values in the order of 5 W K^{-1} m^{-1} with the hybrid-based material displaying once again the best performance. Considering the solvent-free and industrially-compatible production method utilized to manufacture these nanocomposites, the proposed multifunctional materials can expand the range of applications of PHAs and increase the environmental sustainability of the plastic and plastic electronics industry.

Keywords: thermoplastic biopolymer; graphene; carbon nanofibers; electromagnetic interference shielding; thermal dissipation; melt processing

1. Introduction

Plastics are fundamental materials in sectors as diverse as packaging, construction, automotive, electronics, medicine, and sports. Today, a world without synthetic polymers appears unthinkable.[1] Their massive success is driven by their low cost, diverse properties, low maintenance, prolonged lifetime and versatile manufacturing.[2] Most of the existing polymers are constituted by monomers derived from oil, coal or gas.[3] Due to the non-renewable nature of these resources and the longevity of the synthetic plastics, the urge for green alternatives is becoming a priority.[4] In addition, plastics waste management is highly complex considering that several million tons of polymer debris are burned after disposal, producing toxic gases[5] and, as such, contribute to environmental pollution when disposed incorrectly.[6] As a result, bio-based and/or biodegradable plastics, were proposed as a sustainable alternative to synthetic and long-lasting polymers.[2]

Bio-based polymers extracted from renewable biomass sources (e.g. cellulose, starches, sugars from cane and beats, etc.) can reduce the use of fossil fuels. Additionally, biodegradable plastics can degrade in the environment and thus reduce environmental pollution, also contributing positively to the ubiquitous microplastic problem.[7] Among them, the most promising to replace fossil-derived polymers are thermoplastics such as thermoplastic starches (TPS) and polylactic acid (PLA) because of their melt processability. The TPS are bio-based and biodegradable but have a low melting temperature (≈ 60 ºC), high vapor permeability, and poor mechanical properties that are often improved by blending with other polymers.[8] On the other hand, PLA displays a higher melting temperature (≈ 150 - 170 ºC)[9] and better mechanical characteristics but is not biodegradable and needs specialized facilities for composting.[10] There is therefore still a strong need to expand the use of thermoplastic bio-based and/or biodegradable biopolymers.

Polyhydroxyalkanoate (PHA) is a thermoplastic biopolymer produced by the fermentation of glucose-rich materials, volatile fatty acids or organic waste, performed by bacteria and exemplifies a great opportunity to boost the applications of biopolyesters.[11] It is bio-based and biodegradable and given the fact that more than 150 different PHA monomers have been documented, it displays a huge potential to diversify into a large variety of physically and chemically different types of biopolymers, depending on the combination of monomer units.[12] For example, by changing the monomer composition, the melting temperature of PHAs can vary between 40 to 180 °C, the glass transition temperatures can range from -50 to 4 °C and significant variations have been measured also in terms of the degradation temperature, oxygen transmission rate, Young's modulus and tensile strength.[13, 14] Furthermore, PHAs are resistant to ultraviolet light and can be employed in piezoelectric applications.[13, 14] The most popular type of PHA is polyhydroxybutyrate (PHB) which is the simplest (i.e. a single monomer). It is, however, a mechanically weak form of this biopolyester and has manufacturing limitations since its thermal degradation begins a few degrees above its melting temperature.[12, 15] Although some companies recently launched innovative PHA-based polymer grades that can also reduce the overall cost of the

biopolymer,[16] due to its biocompatibility and non-toxicity and its relatively poor thermal and mechanical properties, PHA-using applications are mostly limited to the cosmetic, packaging, drug delivery, and tissue engineering sectors.[13, 17]

An expansion of the applications of PHAs can be achieved by developing composites/nanocomposites where PHAs are used as the polymer matrix.[18] As a result of this procedure, some of the drawbacks of PHAs can be tackled and multifunctional features can be acquired. The most popular strategies to realize composites/nanocomposites based on PHA relies on coupling it with other polymers/biopolymers,[19, 20] fibers,[21] nanoclay,[20, 22] and nanocellulose[23, 24] with the prevalent intention of improving their mechanical behaviour, gas barrier properties, and thermal stability. Other promising nanofillers are carbon-based ones that show the ability to enhance the intrinsic properties of polymers and, at the same time, add new functionalities to a matrix especially when hybrid nanofillers are included, to take advantage of any additive or synergistic effects.[25] Amongst them, carbon nanotubes (CNTs) have been the most utilized and were mostly solvent mixed with PHAs targeting applications in tissue engineering.[26-28] A few studies reported melt blending of PHA with CNTs[29] and some of the targeted applications of these nanocomposites included conductors for electronics.[29, 30]

Other carbon-based nanomaterials such as graphene-related materials (GRMs) or carbon nanofibers (CNFs) have been less commonly used to boost the properties of PHAs although these nanofillers are nowadays produced in large scale and are usually cheaper than CNTs. Amongst GRMs, graphene nanoplatelets (GNPs) are an ideal candidate for the polymer industry in light of their low price (less than 0.1 $/g compared to a few $/g for CNFs), the large volume of production and competitive performances.[31] When GRMs or CNFs were coupled with PHAs, solvent processing was the most common blending technique [32-34] for the production of nanocomposites targeting biomedical applications [33]. As a result, there is still the need for further enhancing the properties of PHAs and expanding the applications of these biopolymers into fields such as electronics[32, 34] or thermal dissipation. Another important breakthrough will be to demonstrate that a simple, scalable, solvent-free and eco-friendly manufacturing processes can be used to manufacture PHAs nanocomposites and that nanofillers such as GNPs and CNFs are a good candidate to fill the performance gap between PHAs and other biopolymers/polymers.

Herein, melt processing was employed to mix PHAs with GNPs or GNPs-CNFs hybrids in an attempt to obtain multifunctional nanocomposites. The thermal stability of the nanocomposite was increased because of the presence of the nanofillers. Additionally, the mechanical properties of the nanocomposites were satisfactory, showing a great improvement in terms of stiffness. The PHA matrix became an electrical conductor with the introduction of both types of nanofillers, with the GNPs-CNFs biocomposite displaying higher electrical conductivity than the GNP-based sample due to the CNFs high aspect ratio. The electromagnetic interference (EMI) performance of the composites was also tested to demonstrate a potential application of these materials, related to their electrical conductivity.

Finally, the thermal conductivity was tested using the Angstrom method and the results were compared to a number of literature reports on GNP-reinforced polymers. The manufactured biocomposites could expand the applications of PHA-based materials into electronics such as in EMI shielding materials, thermally dissipative and structural materials while increasing at the same time the environmental sustainability of the plastic industry.

2. Materials and Methods

PHA was acquired from Goodfellow (grade: Ecomann EM50000, density 1.22 g/cm^3, melting point 110-130 °C, melt flow rate = 2.0 at 170 °C). GNPs were obtained from XG Sciences (grade M25) and were fully characterized (lateral size 7.7 μm, thickness of 6-8 nm) in a previous report[35]. Graphitized CNF (diameter ≈ 100 nm, length between 20 and 200 μm) was purchased from Sigma‐Aldrich (grade PR‐25‐XT‐HHT from Pyrograf Products Inc.) and have also been characterized in an earlier work.[36]

The nanocomposites were melt blended in an internal mixer, Thermo Fisher HAAKE Rheomix, at 130 °C and at 50 rpm for 7 min; the extrudates were subsequently shaped into films by compression molding at 130 °C under a pressure of 30 bar for 5 minutes. Thin films of about 1 mm thickness were created. The production of nanocomposites by melt mixing meant that the use of solvents could be avoided, improving the eco-friendly nature of the material. The GNP weight fractions in the PHA-GNP set of samples was 2.5, 5, 7.5, 10 and 15 wt.%, while the same fractions were used for the PHA-Hyb set of samples, where the ratio between the GNPs and the carbon nanofibers was 1:1 by weight.

Thermogravimetric analysis (TGA) was carried out on a TA Instruments Q5500 TGA. The data was obtained by averaging triplicate samples ran under a nitrogen atmosphere at a heating rate of 10°C min^{-1} to 800 °C.

The stress-strain curves of the samples were obtained using dumbbell-shaped specimens in an Instron 4301 machine, using a load cell of 5 kN and under a tensile rate of 50 mm min^{-1}.

SEM images of the morphology and of the cross section of the specimens were obtained with a Zeiss Evo50 microscope (acceleration voltage of 10 kV). For the cross-sectional SEM pictures, the samples were fractured after being frozen in liquid nitrogen.

The impedance of the bio-nanocomposites was measured on specimens of 10 mm × 10 mm × 1 mm in the in-plane direction. All the measurements were undertaken on a PSM 1735 Frequency Response Analyzer from Newtons4th Ltd connected with Impedance Analysis Interface (IAI). The frequency of alternating current for the measurement were at a range of 1 to 10^6 Hz. The specific conductivity (σ) of composites were calculated from the impedance by the equation:

$$\sigma(\omega) = \frac{1}{Z^*} \times \frac{t}{A} \quad (3)$$

where Z^* is the complex impedance, t is the thickness of specimens (1 mm in this case), A is the area of specimens (10 mm × 10 mm).

The EMI shielding effectiveness of the samples was tested using a vector network analyser (Keysight N5227A) and two WR-90 (8.2-12.4 GHz) waveguide. The transmittance was measured between 8 and 12 GHz.

The in-plane thermal diffusivity of the samples were measured by a custom-built system (scheme of the measuring setup in Figure S1a) using a pulsed (1 Hz) tuneable laser beam and high resolution infrared camera (FLIR T660) mounted with a IR micro lens with a resolution of 50 μm. The laser was used to locally generate periodic heat waves that propagate in the material and are recorded by the infrared camera (Figure S1 b-e). Thermal diffusivity is then calculated following the Angstrom method.[37] For each sample eight measurements were performed along the X and Y axis. A detailed description of the Angstrom method is given in the supporting information (see figure S2).

Heat capacities were obtained from modulated DSC runs on a TA Instruments Q100 DSC for samples weighing 3 to 6 mg, ran in triplicate and averaged. The heat capacity at 25 °C was extracted using TA Universal Analysis software. The samples were heated from -50 to 180 °C at 3°C min^{-1} with a modulation amplitude of 0.5°C min^{-1} and a period of 60 s. The heat capacities (C_p) and the densities (ρ) were used to convert the thermal diffusivity (T_D) into thermal conductivity (κ) using equation:

$$T_D = \frac{K}{\rho C_p} \quad (2).$$

All the above mentioned measurements were performed on at least three specimens unless specified differently.

3. Results and Discussion

3.1 Thermal Stability and Morphology

Thermogravimetric analysis (TGA) revealed a degradation temperature of ~ 275°C in nitrogen for the pure PHA, while the inclusion of nanofillers had a positive effect on the thermal stability of the nanocomposites as shown in Figure 1. Pure PHA has an onset degradation temperature ($T_{5\%}$) of 267± 2 °C and a $T_{50\%}$ of 276 ± 2 °C while the addition of 15 wt.% nanofillers in the form of GNPs or hybrid GNPs-CNFs increases $T_{5\%}$ to 279 ± 1 °C and 277 ± 1 °C, and $T_{50\%}$ to 289.4 ± 0.9 °C and to 287 ± 1 °C, respectively. This indicates that both GNPs and CNFs provide a substantial increase in the thermal stability of the nanocomposites without a significant difference between them. Generally, the higher loadings of GNPs provide superior thermal stability compared to the hybrids, suggesting that higher loadings of high aspect ratio materials provide a greater barrier to the diffusion of degradation

products.[38] It should be pointed out that the mass loss in this temperature region should be attributed to the decomposition of the biopolymer and when higher filler loadings are incorporated, the mass loss of the polymer within the composite can increase significantly, as was reported recently by Kashi *et al.*[39] Herein, the thermal degradation was calculated considering the weight change of the whole nanocomposite sample.

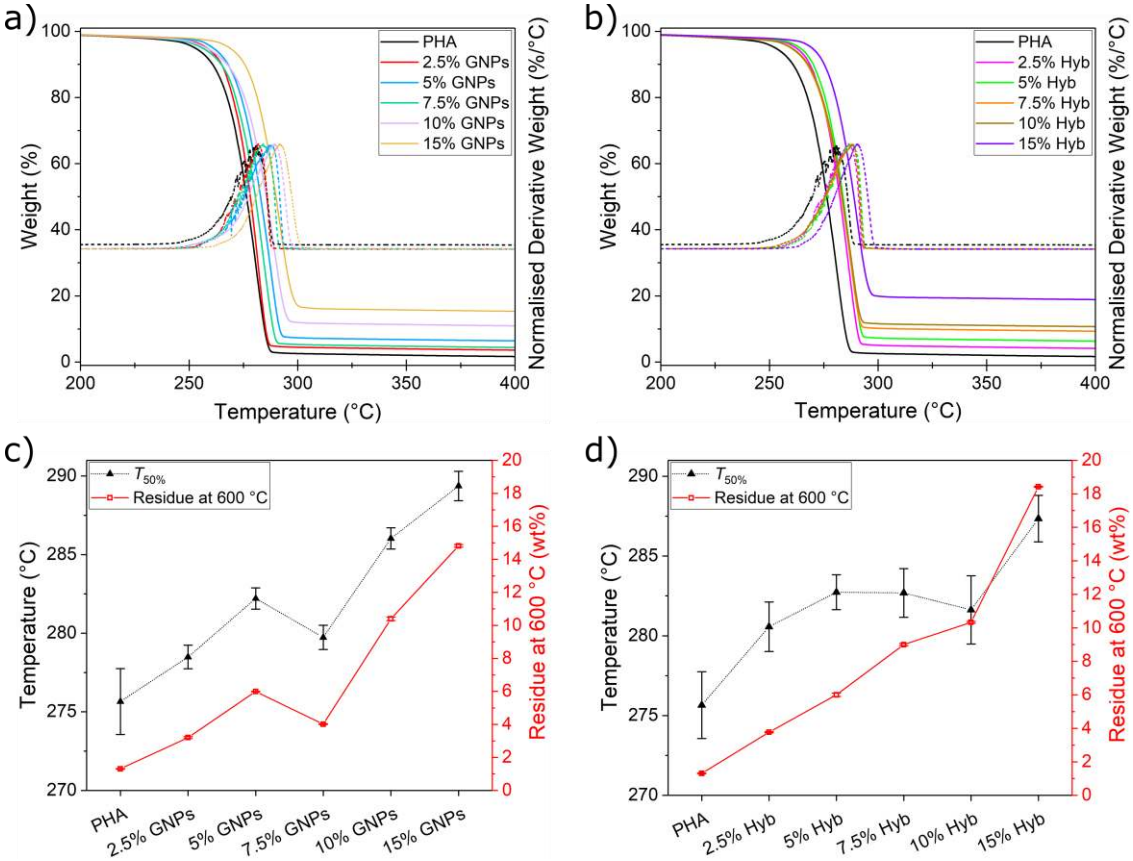

Figure 1: Thermal gravimetric analysis of the PHA nanocomposites displaying weight loss and differential thermogravimetry profiles for a) GNP-based nanocomposites and b) hybrid nanocomposites, along with the variation of $T_{50\%}$ and residue at 600 °C for c) GNP-based nanocomposites and d) hybrid nanocomposites.

Pristine PHA samples macroscopically were rigid and pale yellow in color (inset of Figure 2a) with smooth and uniform surface topographies at the micrometer scale, as displayed in Figure S3. The thickness of all the samples was about 1 mm (see Figure S3). The neat PHA polymer exhibited a regular cross-section with no air bubbles/holes visible through the section (Figures 2a S3). The nanofillers were homogeneously dispersed within the polymer matrix (Figures 2b and 2c). The GNPs-based nanocomposites exhibited the roughest surface (Figure 2b) with roughness increasing with GNPs loading (Figure S4) and a higher amount of restacked flakes and agglomerates.[40] The presence of CNFs can be identified in the hybrid sample presented in Figure 2c, (see Figure S4), while the distribution of

both fillers seems to be more homogeneous. The polymer-filler interface for most of the flakes in both samples appeared to be intact, without the presence of any gaps or voids; this fact is expected to maximize the reinforcement efficiency. Additionally, a small number of flakes can be seen to have folded because of the melt-mixing procedure within the internal mixer. This phenomenon is commonly observed when GNPs are mixed with low-modulus elastomers under high shear rates.[41] Finally, it is interesting to observe that the compression molding procedure that took place after mixing, contributed to a preferred orientation to both the GNPs and the CNFs in the axial direction of the samples. In this case, even if the degree of orientation is not very high, it is expected to contribute to enhanced in-plane mechanical properties and activation of the conduction mechanisms.

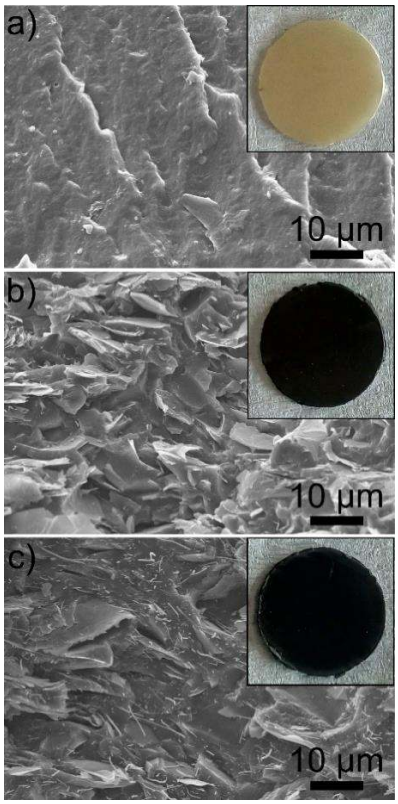

Figure 2: a), b) and c) display the cross-section SEM image of the pure PHA, of the 15 wt.% GNPs sample and of the 15 wt.% hybrid, respectively. Insets shows the photograph of the samples (diameter of the disk around 2.5 cm).

3.2 Mechanical Properties

The mechanical properties of the samples were evaluated by tensile testing and the resulting stress-strain curves are shown in Figure 3a,b. The presence of the nanofillers greatly enhanced the modulus of the matrix by almost doubling it at the highest filler content (15 wt.% or ~ 9 vol%) (Figure 3c,d). The samples were labeled as xGNP or xHyb were x indicates the weight percent of the nanofillers inside the PHA matrix and GNP or Hyb indicate if the nanofiller was pure nanoflakes or the hybrids of GNPs and CNFs, respectively. The super-linear increase of the modulus of the nanocomposites at loadings higher than 5 wt.% (3 vol%) indicates that the fillers exert an additional enhancement at higher filler

contents, as a result of the simultaneous contribution from both individual nanoplatelets and pair of fillers.[41] The two types of fillers seem to have acted additively towards the improvement of the mechanical properties of the bio-nanocomposites similar to what we have seen in hybrid composites where GNPs were combined with carbon fibres[42] and glass fibres[43]. Regarding the tensile strength, it can be seen from Figure 3d that the combination of both CNFs and GNPs hardly altered the behavior of the nanocomposites, while the presence of only GNPs reduced the strength of the matrix. Given that the tensile strength is generally more sensitive to aggregation compared to the modulus of polymer nanocomposites[44], it can be concluded that the samples filled with only GNPs displayed a higher amount of aggregates compared to the hybrid samples. Finally, as expected, the presence of the nanofillers in both types of composites reduced the elongation to failure of the PHA matrix.

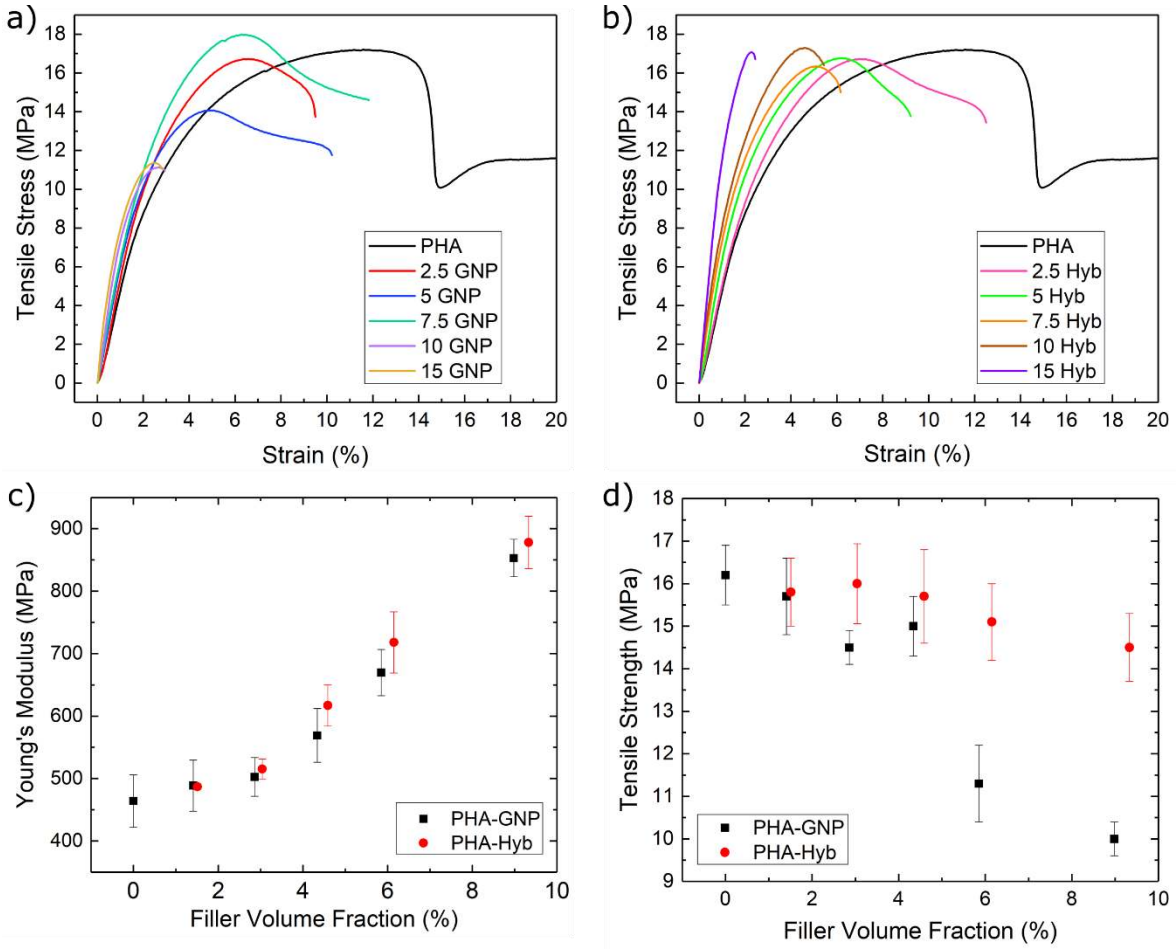

Figure 3: Stress-strain curves of PHA samples filled with a) GNPs and b) Hybrid (GNP-CnF) nanofillers. The results of c) the Young's modulus and d) tensile strength for both types of bio-nanocomposites

3.3 Electrical conductivity

The inclusion of conductive nanofillers can increase the electrical conduction of polymer composites.[45, 46] Figures 4a-b show the specific electrical conductivity as a function of the frequency of the input current for the GNP- and Hyb-based samples, respectively. Low conductivities defining an insulating behaviour, were measured for the pure PHA biopolymer and for the GNP-based samples up to 7.5 wt.%

loadings (Figure 4a). In contrast, the specific electrical conductivity increased by about nine orders of magnitude at 10 wt.% GNPs loading. This suggests that the electrical percolation threshold, defined as the loading at which the conductive nanofillers form efficiently interconnected conductive pathways,[47] takes place between 7.5 and 10 wt.% loading of GNPs. After percolation, the electrical conductivity increased, reaching values of ~ 0.1 S/m and ~ 0.3 S/m for nanocomposites filled with 10 wt.% and 15 wt.% of GNPs, respectively. A lower percolation threshold was detected for the hybrid-based nanocomposites, as shown in Figure 4b. Indeed, the electrical conductivity improved of five orders of magnitude at 1 Hz frequency when the concentration of the hybrid fillers increased from 5 wt.% to 7.5 wt.%, suggesting that percolation occurred in between these two loadings. After percolation, the electrical conductivity increased with increasing filler content, reaching values of ~ 0.1 S/m and ~ 2 S/m for 10 wt.% and 15 wt.% loadings, respectively. It is worth noticing that at the highest nanofillers loading, the Hyb-based biocomposite displays an electrical conductivity that is ~ 6 times higher than the GNP-based sample at the same loading. This is due to the higher number of connections between nanofiber-nanoflakes in the hybrid samples compared with the pure GNPs specimen.[25, 31] This work is the first to report the electrical percolation study of a PHA-GNP nanocomposite produced by melt mixing. Recently, Papadopoulou *et al.* [34] solvent-blended PHB with GNPs finding a percolation threshold of 7 wt. %. Another work by Yao *et al.* [32] describes the production of solution processed PHA-graft-graphene composites with a percolation threshold of 0.5 wt %. These two are the only two reports that deal with electrical percolation threshold of graphene PHA composites. In our case, the percolation threshold was found between 5 and 7.5 wt % for the hybrid nanocomposites and between 7.5 and 10 wt % for the GNP-only filled samples, in line with the results previously reported by Papadopoulou *et al.* but by avoiding the use of an organic solvent to mix the polymer and the fillers. The conductivities obtained reveal the possibility of exploitation of these eco-friendly materials in applications such as electromagnetic interference shielding (seen later in Figure 5), structural health monitoring[48] and electrodes for tactile/pressure sensors [31, 36].

Both pure GNP and Hyb biocomposites showed a two-phase capacitive and/or resistive structure behavior.[49] Before the percolation threshold, a dielectric behavior was measured with the conductivity being linearly dependent on the frequency (capacitive state). In contrast, above percolation the electrical conductivity remained constant with increasing frequency, determining the formation of a conductive network in the biopolymer matrix (resistive behavior). Where the conductivity exhibited a linear dependence on frequency the predominant mechanism was capacitive behavior for the low filler loadings (i.e. before electrical percolation). The prevalence of the resistive component at high filler loading implies the formation of effective percolation networks. The 7.5 wt.% Hyb sample displayed resistive performance at low frequencies (with electrical conductivity independent on frequency) and a switch to capacitive behavior at frequencies around 105 Hz, indicating that the conductive networks are not yet fully formed at this filler loading.

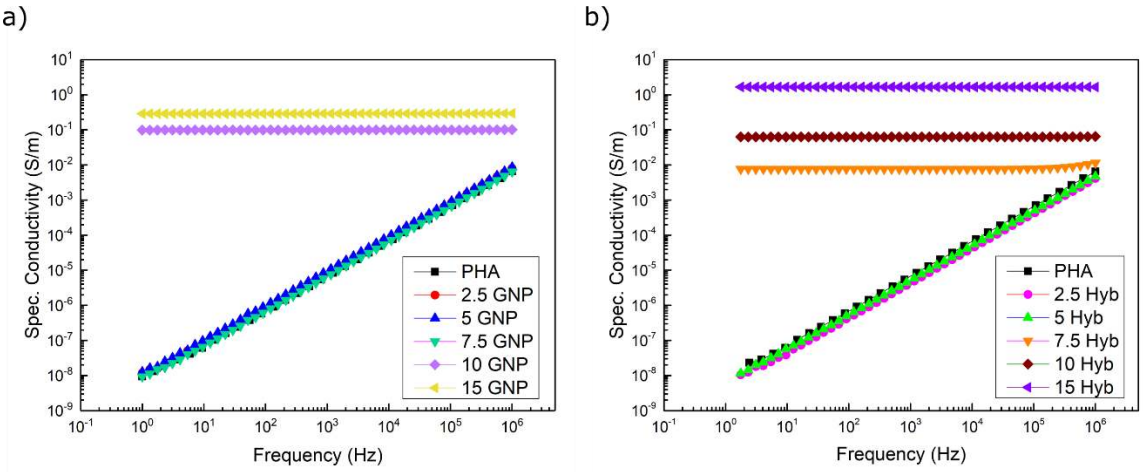

Figure 4: Graph of electrical conductivity as a function of frequency for GNP (a) and (b) Hyb (1:1 GNP to CNF ratio) samples.

3.4 Electromagnetic Interference Shielding

Electrical devices are generally designed as arrays of densely packed electronic components.[50] As a result, the generation of EMI can lead to failure of the expected operation of electrical instruments caused by the crosstalk of adjacent electronic units.[51] Consequently, effective EMI shielding is crucial to safeguard the optimal performance of electronics.[52] Metals are commonly used for EMI shielding although they are mechanically rigid, corrosion-prone and expensive.[53, 54] Recently, conductive nanofiller-reinforced biopolymers have been suggested as an eco-friendly alternative to eliminate and control EMI. [50, 53] Herein, we tested the EMI shielding performance of the GNP- and Hyb-based biocomposites as a function of nanofiller content. The EMI shielding ,was measured at frequencies between 8 and 12 GHz (X-band), which are the most common frequencies for the operation of consumer electronics.[55] During EMI shielding an electromagnetic wave is reflected, absorbed and transmitted when it passes through a conductor. The larger the electromagnetic screening, the lower the amplitude of the transmitted wave.

Figure 5 displays the transmittance (ratio between the transmitted and the incident electromagnetic power) as a function of the frequency of the incident electromagnetic waves for GNP- based samples with different nanoflake concentrations. As can be seen, increasing the nanofiller concentration enhances the electromagnetic shielding effect. The screening efficiency was found to improve of approximately -1.04 dB per wt.% of GNPs, as shown in Figure S5. The 10 and 15 wt.% GNP-based samples revealed a transmittance of approximately -11.2 and -15.4 dB, respectively. The inclusion of the nanofillers produced an enhancement of the SE also for the composites containing the hybrid fillers, with an improvement of -1.4 dB per unit wt.% of nanofillers, as shown in Figure S5. The 10 and 15 wt.% Hyb-based samples showed a transmittance of approximately -14.6 and -22.7 dB, respectively. These values are approximately 30% and 50% higher compared to the GNP-based samples loaded with the same filler amounts. This result agrees with the lower electrical resistance that the Hyb samples

showed compared to the composites with GNPs, as shown in Figure 4. In general, the X-band EMI shielding effectivenesses reported herein, are comparable to other similar literature works on PMMA-GNP nanocomposites [56] or epoxy-GNP nanocomposites [57]. It is worth noticing that the 15 wt.% Hyb samples display shielding effectiveness higher than 20 dB, which is the threshold for numerous commercial applications.[50, 53, 55]

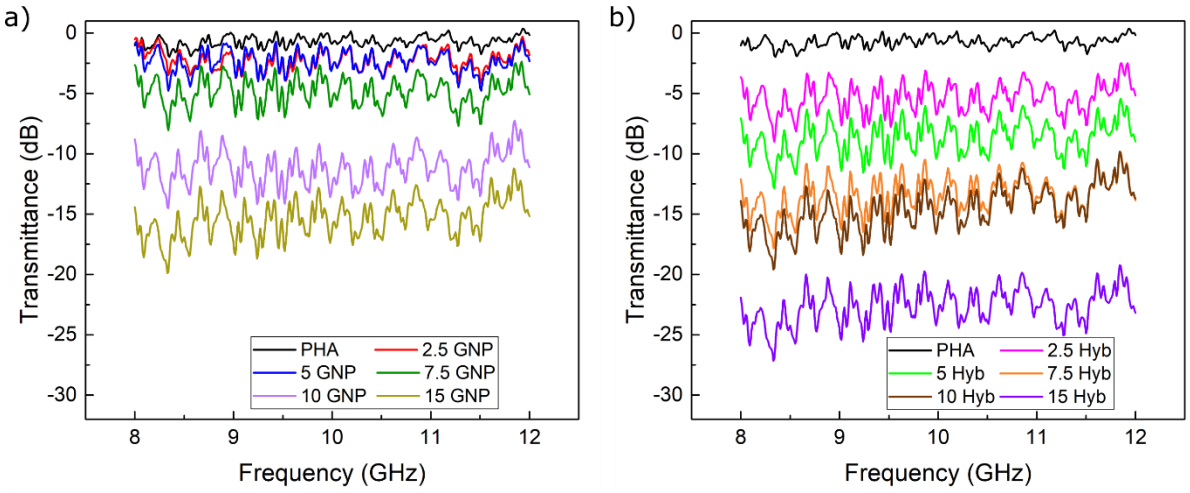

Figure 5: Transmittance of the biocomposites between 8 and 12 GHz. a) and b) GNP- and hybrid-based composites, respectively.

3.5 Thermal Dissipation Properties

Another important issue in electronic devices is the heat generated by their resistive components due to the Joule effect. Such heating effects are increasing due to the constantly growing density of microprocessors of personal computers and smartphones (according to the trend predicted by Moore's law) and the resulting enlarged power consumption of the electronics components.[58] Often, thermal dissipation concerns are coupled with EMI shielding dysfunction due to the abovementioned proximity of electrically conductive elements and their interference.[51] The possibility to solve both problems at once by employing eco-friendly materials could constitute a great advantage for electronics manufacturers.[51, 59] Hence, we measured the thermal diffusivity (TD), the rate at which one material is able to transfer heat, and we extracted the thermal conductivity of the GNP- and Hyb- based biopolymers, as shown in Figure 6. The neat PHA matrix displayed a TD of 0.15 mm^2/s (Figure 6a), a quite typical value for the majority of polymers due to their amorphous structure.[60] At low filler content, the fillers are located at a distance from one another, not forming a percolating network. With increasing loading of GNPs, the thermal diffusivity continued to increase, almost exponentially, reaching values of 0.53 and 1.16 mm^2/s at 10 and 15 wt.% nanoflakes concentrations, approximately 250% and 670% higher than the bare biopolymer, respectively. The inclusion of the hybrid nanofillers resulted in an even more evident improvement of the thermal diffusivity, as shown in Figure 6b. Indeed, at 10 and 15 Hyb samples TD reached values of 0.75 and 1.38 mm^2/s, an increase of 500% and 920%, respectively. The diffusivity is greatly enhanced with increasing mass fractions of the nanofillers but especially at 15

wt.% (around 9 vol%) of either GNPs or the Hyb filler, as a result of the creation of thermally conductive pathways inside the biopolymer. Especially for the case of the hybrid 1D-2D nanofillers, the carbon nanofibers with their exceptionally high aspect ratio can bridge the GNPs, thus creating highly conductive graphene-graphene networks. Regarding the thermal conductivity of the samples, the increase of thermal conductivity was impressive for both types of composites, with the rate of increase being exponential and the maximum conductivity at the highest filler contents (around 9 vol%) being 1750% higher for the GNP-filled PHA and 1930% higher for the Hyb-filled PHA (Figures 7c and 7d). These values are in the same range of the vast majority of commercially available thermal interface materials, which display thermal conductivities in the range of 0.5-10 $Wm^{-1}K^{-1}$, generally achieved at very high filler volume fractions of around 50 vol% [61] (that is almost 5 times higher than the filler contents used in this work). These values are comparable with state-of-the-art thermal conductivity obtained using other carbon-based nanofillers inside the polymer matrix (see Table 1).

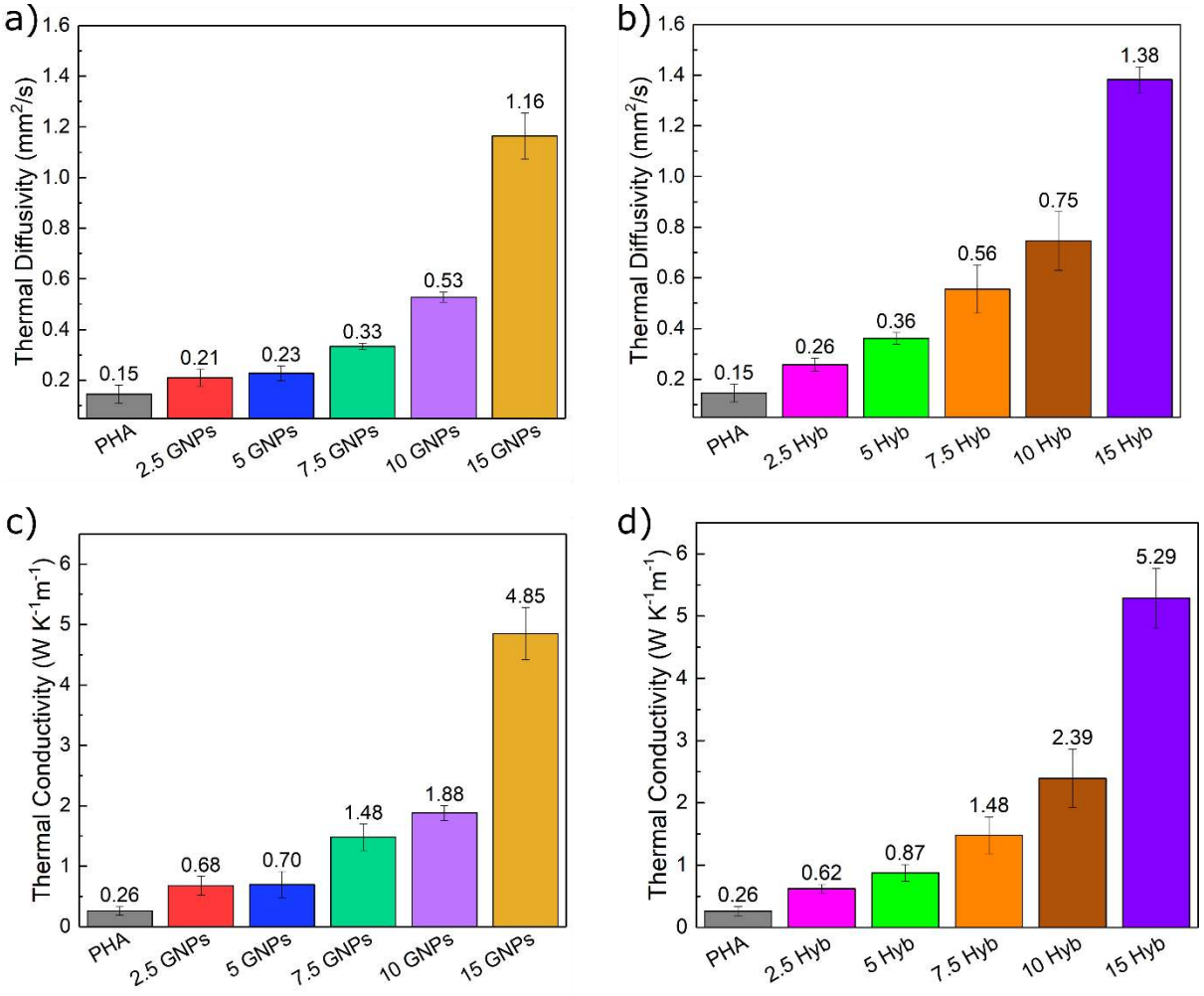

Figure 6: Thermal diffusivity of the bio-nanocomposites filled with (a) GNPs and (b) hybrid, binary GNP-CnF fillers as a function of nanofiller weight fraction (wt.%). Thermal conductivity of the nanocomposites filled with (c) GNPs and (d) hybrid GNP-CnF (Hyb) fillers.

Table 1: Thermal conductivity of selected nanocomposites that employ carbon-based nanofillers.

Sample	Nanofiller load (vol.%)	Method	Thermal Conductivity (W K-1 m-1)	Reference
GNP-epoxy	6	Infrared thermography	0.6	[62]
GNP-epoxy	25	Steady state method	6. 9	[63]
GNP-Epoxy	10	Laser flash	5.1	[61]
GNP/CNT-epoxy	0.6	Hot disk	0.3	[64]
GNP-epoxy	24	Steady state method	6.5	[65]
GNP-epoxy	45	Hot disk	11.0	[66]
GNP-epoxy	1.2	Laser flash	0.5	[67]
CNF-rubbery epoxy	31.6	Hot disk	1.9	[68]
GNP-polycarbonate	12	Hot disk	7.3	[69]
CNT-polydimethylsiloxane	1.8	ASTM method	1.8	[70]
GNP/CNF-PHA	9.0	Angstrom Method	5.3 ± 0.3	This work

4. Conclusions

In pursuit of enhancing its features and achieving multifunctionality, a PHA biopolyester was melt blended with GNPs or hybrids of GNPs and CNFs. GNPs were preferred compared to CNFs since they are high-performing, cheap, and multifunctional nanofillers that can be easily produced and manipulated on a large scale. The inclusion of nanofillers increased the thermal stability of the nanocomposites by ~10°C. At the highest nanoparticle loading (15 wt.%), the Young's modulus of the matrix roughly doubled while the tensile stress decreased only around 10% and 40% for the hybrids and GNPs reinforced samples, respectively. The hybrid nanocomposites displayed electrical percolation at filler content between 5 and 7.5 wt.%, whereas the pure GNP-based samples became conductive at loadings between 7.5 and 10 wt.%. The electrical conductivity of the biopolymer increased considerably, with the best performance obtained using 15 wt.% of the hybrid filler that was ~ 6 times higher compared to the GNP-based sample at the same loading. As a result, the EMI shielding performance of the hybrid nanocomposites was 50% higher than the GNPs samples and displayed shielding effectiveness > 20 dB, which is the threshold for commercial applications. The thermal conductivity increased significantly for both types of bio-nanocomposites and reached values around 5 W K-1 m-1, with the maximum conductivity at the highest filler content being 1750% and 1930% higher than the pure PHA matrix in for the pure GNP- and hybrid-based nanocomposites case, respectively. The multifunctional materials developed show very promising multifunctional properties, they can expand the range of application of PHA biopolymers and increase the environmental sustainability of the plastics industry.

Acknowledgements
This project has received funding from the European Union's Horizon 2020 research and innovation programme under grant agreement No 785219.

Supporting Information. SEM high magnification images, EMI shielding analysis and details on the setup used to measure the thermal conductivity of the materials are provided.

References

1. Geyer, R.; Jambeck, J. R.; Law, K. L., Production, use, and fate of all plastics ever made. *Science advances* **2017,** *3* (7), e1700782.
2. Mekonnen, T.; Mussone, P.; Khalil, H.; Bressler, D., Progress in bio-based plastics and plasticizing modifications. *Journal of Materials Chemistry A* **2013,** *1* (43), 13379-13398.
3. Albuquerque, P. B.; Malafaia, C. B., Perspectives on the production, structural characteristics and potential applications of bioplastics derived from polyhydroxyalkanoates. *International journal of biological macromolecules* **2018,** *107*, 615-625.
4. Soroudi, A.; Jakubowicz, I., Recycling of bioplastics, their blends and biocomposites: A review. *European Polymer Journal* **2013,** *49* (10), 2839-2858.
5. Yamada-Onodera, K.; Mukumoto, H.; Katsuyaya, Y.; Saiganji, A.; Tani, Y., Degradation of polyethylene by a fungus, Penicillium simplicissimum YK. *Polymer degradation and stability* **2001,** *72* (2), 323-327.
6. Jambeck, J. R.; Geyer, R.; Wilcox, C.; Siegler, T. R.; Perryman, M.; Andrady, A.; Narayan, R.; Law, K. L., Plastic waste inputs from land into the ocean. *Science* **2015,** *347* (6223), 768-771.
7. Magrì, D.; Sánchez-Moreno, P.; Caputo, G.; Gatto, F.; Veronesi, M.; Bardi, G.; Catelani, T.; Guarnieri, D.; Athanassiou, A.; Pompa, P. P., Laser ablation as a versatile tool to mimic polyethylene terephthalate nanoplastic pollutants: characterization and toxicology assessment. *ACS nano* **2018,** *12* (8), 7690-7700.
8. Zhang, Y.; Rempel, C.; McLaren, D., Thermoplastic starch. In *Innovations in food packaging*, Elsevier: 2014; pp 391-412.
9. Cataldi, P.; Bayer, I. S.; Nanni, G.; Athanassiou, A.; Bonaccorso, F.; Pellegrini, V.; Castillo, A. E. D.; Ricciardella, F.; Artyukhin, S.; Tronche, M. A.; Gogotsi, Y.; Cingolani, R., Effect of graphene nano-platelet morphology on the elastic modulus of soft and hard biopolymers. *Carbon* **2016,** *109*, 331-339.
10. Gorrasi, G.; Pantani, R., Effect of PLA grades and morphologies on hydrolytic degradation at composting temperature: assessment of structural modification and kinetic parameters. *Polymer degradation and stability* **2013,** *98* (5), 1006-1014.
11. Melendez-Rodriguez, B.; Castro-Mayorga, J. L.; Reis, M. A.; Sammon, C.; Cabedo, L.; Torres-Giner, S.; Lagaron, J. M., Preparation and characterization of electrospun food biopackaging films of poly (3-hydroxybutyrate-co-3-hydroxyvalerate) derived from fruit pulp biowaste. *Frontiers in Sustainable Food Systems* **2018,** *2*, 38.
12. Chanprateep, S., Current trends in biodegradable polyhydroxyalkanoates. *Journal of bioscience and bioengineering* **2010,** *110* (6), 621-632.
13. Raza, Z. A.; Abid, S.; Banat, I. M., Polyhydroxyalkanoates: Characteristics, production, recent developments and applications. *International Biodeterioration & Biodegradation* **2018,** *126*, 45-56.
14. Bugnicourt, E.; Cinelli, P.; Lazzeri, A.; Alvarez, V. A., Polyhydroxyalkanoate (PHA): Review of synthesis, characteristics, processing and potential applications in packaging. **2014**.
15. Ray, S.; Kalia, V. C., Co-metabolism of substrates by Bacillus thuringiensis regulates polyhydroxyalkanoate co-polymer composition. *Bioresource technology* **2017,** *224*, 743-747.

16. Chen, G.-Q., Industrial production of PHA. In *Plastics from bacteria*, Springer: 2010; pp 121-132.
17. Degli Esposti, M.; Chiellini, F.; Bondioli, F.; Morselli, D.; Fabbri, P., Highly porous PHB-based bioactive scaffolds for bone tissue engineering by in situ synthesis of hydroxyapatite. *Materials Science and Engineering: C* **2019,** *100*, 286-296.
18. Sun, J.; Shen, J.; Chen, S.; Cooper, M. A.; Fu, H.; Wu, D.; Yang, Z., Nanofiller reinforced biodegradable PLA/PHA composites: Current status and future trends. *Polymers* **2018,** *10* (5), 505.
19. Gumel, A.; Annuar, M., Nanocomposites of polyhydroxyalkanoates (PHAs). *Polyhydroxyalkanoate (PHA) Based Blends, Composites and Nanocomposites* **2014**, 98-118.
20. González‐Ausejo, J.; Gámez‐Pérez, J.; Balart, R.; Lagarón, J. M.; Cabedo, L., Effect of the addition of sepiolite on the morphology and properties of melt compounded PHBV/PLA blends. *Polymer Composites* **2019,** *40* (S1), E156-E168.
21. Zhao, C.; Li, J.; He, B.; Zhao, L., Fabrication of hydrophobic biocomposite by combining cellulosic fibers with polyhydroxyalkanoate. *Cellulose* **2017,** *24* (5), 2265-2274.
22. García-Quiles, L.; Cuello, Á. F.; Castell, P., Sustainable Materials with Enhanced Mechanical Properties Based on Industrial Polyhydroxyalkanoates Reinforced with Organomodified Sepiolite and Montmorillonite. *Polymers* **2019,** *11* (4), 696.
23. Martínez‐Sanz, M.; Lopez‐Rubio, A.; Villano, M.; Oliveira, C. S.; Majone, M.; Reis, M.; Lagarón, J. M., Production of bacterial nanobiocomposites of polyhydroxyalkanoates derived from waste and bacterial nanocellulose by the electrospinning enabling melt compounding method. *Journal of Applied Polymer Science* **2016,** *133* (2).
24. Valentini, F.; Dorigato, A.; Rigotti, D.; Pegoretti, A., Polyhydroxyalkanoates/Fibrillated Nanocellulose Composites for Additive Manufacturing. *Journal of Polymers and the Environment* **2019,** *27* (6), 1333-1341.
25. Szeluga, U.; Kumanek, B.; Trzebicka, B., Synergy in hybrid polymer/nanocarbon composites. A review. *Composites Part A: Applied Science and Manufacturing* **2015,** *73*, 204-231.
26. Phan, D. C.; Goodwin Jr, D. G.; Frank, B. P.; Bouwer, E. J.; Fairbrother, D. H., Biodegradability of carbon nanotube/polymer nanocomposites under aerobic mixed culture conditions. *Science of the Total Environment* **2018,** *639*, 804-814.
27. Amaral Montanheiro, T. L.; Montagna, L. S.; Machado, J. P. B.; Lemes, A. P., Covalent functionalization of MWCNT with PHBV chains: Evaluation of the functionalization and production of nanocomposites. *Polymer Composites* **2019,** *40* (1), 288-295.
28. Yu, H.-Y.; Qin, Z.-Y.; Sun, B.; Yang, X.-G.; Yao, J.-M., Reinforcement of transparent poly (3-hydroxybutyrate-co-3-hydroxyvalerate) by incorporation of functionalized carbon nanotubes as a novel bionanocomposite for food packaging. *Composites Science and Technology* **2014,** *94*, 96-104.
29. Vidhate, S.; Innocentini‐Mei, L.; D'Souza, N. A., Mechanical and electrical multifunctional poly (3‐hydroxybutyrate‐co‐3‐hydroxyvalerate)—multiwall carbon nanotube nanocomposites. *Polymer Engineering & Science* **2012,** *52* (6), 1367-1374.
30. Valentini, L.; Fabbri, P.; Messori, M.; Degli Esposti, M.; Bittolo Bon, S., Multilayer films composed of conductive poly (3‐hydroxybutyrate)/carbon nanotubes bionanocomposites and a photoresponsive conducting polymer. *Journal of Polymer Science Part B: Polymer Physics* **2014,** *52* (8), 596-602.
31. Cataldi, P.; Athanassiou, A.; Bayer, I. S., Graphene Nanoplatelets-Based Advanced Materials and Recent Progress in Sustainable Applications. *Appl Sci-Basel* **2018,** *8* (9), 1438.

32. Yao, H.; Wu, L.-p.; Chen, G.-Q., Synthesis and characterization of electroconductive PHA-graft-graphene nanocomposites. *Biomacromolecules* **2018,** *20* (2), 645-652.
33. Pramanik, N.; De, J.; Basu, R. K.; Rath, T.; Kundu, P. P., Fabrication of magnetite nanoparticle doped reduced graphene oxide grafted polyhydroxyalkanoate nanocomposites for tissue engineering application. *Rsc Adv* **2016,** *6* (52), 46116-46133.
34. Papadopoulou, E. L.; Basnett, P.; Paul, U. C.; Marras, S.; Ceseracciu, L.; Roy, I.; Athanassiou, A., Green Composites of Poly (3-hydroxybutyrate) Containing Graphene Nanoplatelets with Desirable Electrical Conductivity and Oxygen Barrier Properties. *ACS Omega* **2019**.
35. Young, R. J.; Liu, M.; Kinloch, I. A.; Li, S.; Zhao, X.; Vallés, C.; Papageorgiou, D. G., The mechanics of reinforcement of polymers by graphene nanoplatelets. *Composites Science and Technology* **2018,** *154*, 110-116.
36. Cataldi, P.; Dussoni, S.; Ceseracciu, L.; Maggiali, M.; Natale, L.; Metta, G.; Athanassiou, A.; Bayer, I. S., Carbon Nanofiber versus Graphene-Based Stretchable Capacitive Touch Sensors for Artificial Electronic Skin. *Adv Sci (Weinh)* **2018,** *5* (2), 1700587.
37. Wu, X.; Steiner, P.; Raine, T.; Pinter, G.; Kretinin, A.; Kocabas, C.; Bissett, M.; Cataldi, P., Hybrid Graphene/Carbon Nanofiber Wax Emulsion for Paper‐Based Electronics and Thermal Management. *Advanced Electronic Materials* **2020**, 2000232.
38. Bao, C.; Song, L.; Xing, W.; Yuan, B.; Wilkie, C. A.; Huang, J.; Guo, Y.; Hu, Y., Preparation of graphene by pressurized oxidation and multiplex reduction and its polymer nanocomposites by masterbatch-based melt blending. *Journal of Materials Chemistry* **2012,** *22* (13), 6088-6096.
39. Kashi, S.; Gupta, R. K.; Kao, N.; Hadigheh, S. A.; Bhattacharya, S. N., Influence of graphene nanoplatelet incorporation and dispersion state on thermal, mechanical and electrical properties of biodegradable matrices. *Journal of materials science & technology* **2018,** *34* (6), 1026-1034.
40. Cataldi, P.; Condurache, O.; Spirito, D.; Krahne, R.; Bayer, I. S.; Athanassiou, A.; Perotto, G., Keratin-Graphene Nanocomposite: Transformation of Waste Wool in Electronic Devices. *ACS Sustainable Chemistry & Engineering* **2019**.
41. Liu, M.; Kinloch, I. A.; Young, R. J.; Papageorgiou, D. G., Modelling mechanical percolation in graphene-reinforced elastomer nanocomposites. *arXiv preprint arXiv:1903.10224* **2019**.
42. Papageorgiou, D. G.; Liu, M.; Li, Z.; Vallés, C.; Young, R. J.; Kinloch, I. A., Hybrid poly (ether ether ketone) composites reinforced with a combination of carbon fibres and graphene nanoplatelets. *Composites Science and Technology* **2019,** *175*, 60-68.
43. Papageorgiou, D. G.; Kinloch, I. A.; Young, R. J., Hybrid multifunctional graphene/glass-fibre polypropylene composites. *Composites Science and Technology* **2016,** *137*, 44-51.
44. Papageorgiou, D. G.; Kinloch, I. A.; Young, R. J., Graphene/elastomer nanocomposites. *Carbon* **2015,** *95*, 460-484.
45. Cataldi, P.; Cassinelli, M.; Heredia‐Guerrero, J. A.; Guzman‐Puyol, S.; Naderizadeh, S.; Athanassiou, A.; Caironi, M., Green Biocomposites for Thermoelectric Wearable Applications. *Advanced Functional Materials* **2019**.
46. Cataldi, P.; Ceseracciu, L.; Athanassiou, A.; Bayer, I. S., Healable Cotton–Graphene Nanocomposite Conductor for Wearable Electronics. *ACS applied materials & interfaces* **2017,** *9* (16), 13825-13830.

47. Stankovich, S.; Dikin, D. A.; Dommett, G. H.; Kohlhaas, K. M.; Zimney, E. J.; Stach, E. A.; Piner, R. D.; Nguyen, S. T.; Ruoff, R. S., Graphene-based composite materials. *Nature* **2006,** *442* (7100), 282-6.
48. Montazerian, H.; Rashidi, A.; Dalili, A.; Najjaran, H.; Milani, A. S.; Hoorfar, M., Graphene‐coated spandex sensors embedded into silicone sheath for composites health monitoring and wearable applications. *Small* **2019,** *15* (17), 1804991.
49. Xia, T.; Zeng, D.; Li, Z.; Young, R. J.; Vallés, C.; Kinloch, I. A., Electrically conductive GNP/epoxy composites for out-of-autoclave thermoset curing through Joule heating. *Composites Science and Technology* **2018,** *164*, 304-312.
50. Cataldi, P.; Heredia‐Guerrero, J. A.; Guzman‐Puyol, S.; Ceseracciu, L.; La Notte, L.; Reale, A.; Ren, J.; Zhang, Y.; Liu, L.; Miscuglio, M., Sustainable Electronics Based on Crop Plant Extracts and Graphene: A "Bioadvantaged" Approach. *Advanced Sustainable Systems* **2018,** *2* (11), 1800069.
51. Kargar, F.; Barani, Z.; Balinskiy, M.; Magana, A. S.; Lewis, J. S.; Balandin, A. A., Dual-Functional Graphene Composites for Electromagnetic Shielding and Thermal Management. *Advanced Electronic Materials* **2019,** *5* (1), 1800558.
52. Mates, J. E.; Bayer, I. S.; Salerno, M.; Carroll, P. J.; Jiang, Z.; Liu, L.; Megaridis, C. M., Durable and flexible graphene composites based on artists' paint for conductive paper applications. *Carbon* **2015,** *87*, 163-174.
53. Cataldi, P.; Bonaccorso, F.; Esau del Rio Castillo, A.; Pellegrini, V.; Jiang, Z.; Liu, L.; Boccardo, N.; Canepa, M.; Cingolani, R.; Athanassiou, A., Cellulosic Graphene Biocomposites for Versatile High‐Performance Flexible Electronic Applications. *Advanced Electronic Materials* **2016,** *2* (11), 1600245.
54. Cataldi, P.; Papageorgiou, D. G.; Pinter, G.; Kretinin, A. V.; Sampson, W. W.; Young, R. J.; Bissett, M.; Kinloch, I. A., Graphene-Polyurethane Coatings for Deformable Conductors and Electromagnetic Interference Shielding. *Advanced Electronic Materials* **2020**.
55. Vallés, C.; Zhang, X.; Cao, J.; Lin, F.; Young, R. J.; Lombardo, A.; Ferrari, A. C.; Burk, L.; Mülhaupt, R.; Kinloch, I. A., Graphene/Polyelectrolyte Layer-by-Layer Coatings for Electromagnetic Interference Shielding. *ACS Applied Nano Materials* **2019,** *2* (8), 5272-5281.
56. Im, H. J.; Oh, J. Y.; Ryu, S.; Hong, S. H., The design and fabrication of a multilayered graded GNP/Ni/PMMA nanocomposite for enhanced EMI shielding behavior. *Rsc Adv* **2019,** *9* (20), 11289-11295.
57. Bhaskaran, K.; Bheema, R. K.; Etika, K. C., The influence of Fe3O4@ GNP hybrids on enhancing the EMI shielding effectiveness of epoxy composites in the X-band. *Synthetic Metals* **2020,** *265*, 116374.
58. Barani, Z.; Mohammadzadeh, A.; Geremew, A.; Huang, C. Y.; Coleman, D.; Mangolini, L.; Kargar, F.; Balandin, A. A., Thermal Properties of the Binary‐Filler Hybrid Composites with Graphene and Copper Nanoparticles. *Advanced Functional Materials* **2019**, 1904008.
59. Zahid, M.; Masood, M. T.; Athanassiou, A.; Bayer, I. S., Sustainable thermal interface materials from recycled cotton textiles and graphene nanoplatelets. *Applied Physics Letters* **2018,** *113* (4), 044103.
60. Xie, X.; Li, D.; Tsai, T.-H.; Liu, J.; Braun, P. V.; Cahill, D. G., Thermal conductivity, heat capacity, and elastic constants of water-soluble polymers and polymer blends. *Macromolecules* **2016,** *49* (3), 972-978.

61. Shahil, K. M.; Balandin, A. A., Graphene–multilayer graphene nanocomposites as highly efficient thermal interface materials. *Nano letters* **2012,** *12* (2), 861-867.
62. Gresil, M.; Wang, Z.; Poutrel, Q.-A.; Soutis, C., Thermal diffusivity mapping of graphene based polymer nanocomposites. *Scientific reports* **2017,** *7* (1), 5536.
63. Yu, A.; Ramesh, P.; Itkis, M. E.; Bekyarova, E.; Haddon, R. C., Graphite nanoplatelet− epoxy composite thermal interface materials. *The Journal of Physical Chemistry C* **2007,** *111* (21), 7565-7569.
64. Yang, S.-Y.; Lin, W.-N.; Huang, Y.-L.; Tien, H.-W.; Wang, J.-Y.; Ma, C.-C. M.; Li, S.-M.; Wang, Y.-S., Synergetic effects of graphene platelets and carbon nanotubes on the mechanical and thermal properties of epoxy composites. *Carbon* **2011,** *49* (3), 793-803.
65. Yu, A.; Ramesh, P.; Sun, X.; Bekyarova, E.; Itkis, M. E.; Haddon, R. C., Enhanced thermal conductivity in a hybrid graphite nanoplatelet–carbon nanotube filler for epoxy composites. *Advanced Materials* **2008,** *20* (24), 4740-4744.
66. Kargar, F.; Barani, Z.; Salgado, R.; Debnath, B.; Lewis, J. S.; Aytan, E.; Lake, R. K.; Balandin, A. A., Thermal percolation threshold and thermal properties of composites with high loading of graphene and boron nitride fillers. *ACS applied materials & interfaces* **2018,** *10* (43), 37555-37565.
67. Chatterjee, S.; Wang, J.; Kuo, W.; Tai, N.; Salzmann, C.; Li, W.-L.; Hollertz, R.; Nüesch, F.; Chu, B., Mechanical reinforcement and thermal conductivity in expanded graphene nanoplatelets reinforced epoxy composites. *Chemical Physics Letters* **2012,** *531*, 6-10.
68. Raza, M. A.; Westwood, A.; Stirling, C., Effect of processing technique on the transport and mechanical properties of vapour grown carbon nanofibre/rubbery epoxy composites for electronic packaging applications. *Carbon* **2012,** *50* (1), 84-97.
69. Kim, H. S.; Bae, H. S.; Yu, J.; Kim, S. Y., Thermal conductivity of polymer composites with the geometrical characteristics of graphene nanoplatelets. *Scientific reports* **2016,** *6*, 26825.
70. Liu, C.; Huang, H.; Wu, Y.; Fan, S., Thermal conductivity improvement of silicone elastomer with carbon nanotube loading. *Applied Physics Letters* **2004,** *84* (21), 4248-4250.